

Silica Nanoparticles Tailored with a Molecularly Imprinted Copolymer Layer as a Highly Selective Biorecognition Element

Zehra Oluz, Mustafa Göktürk Yazlak, Tuğana Talya Kurşun, Sana Nayab, Gunnar Glasser, Basit Yameen, and Hatice Duran*

Molecularly imprinted silica nanoparticles (SP-MIP) are synthesized for the real-time optical detection of low-molecular-weight compounds. Azo-initiator-modified silica beads are functionalized through reversible addition-fragmentation chain transfer (RAFT) polymerization, which leads to efficient control of the grafted layer. The copolymerization of methacrylic acid (MAA) and ethylene glycol dimethacrylate (EDMA) on azo initiator-coated silica particles (≈ 100 nm) using chain transfer agent (2-phenylprop-2-yl-dithiobenzoate) is carried out in the presence of a target analyte molecule (L-Boc-phenylalanine anilide, L-BFA). The chemical and morphological properties of SP-MIP are characterized by scanning electron microscopy, X-ray photoelectron spectroscopy, Brunauer–Emmett–Teller surface analysis, and thermogravimetric analysis. Finally, SP-MIP is located on the gold surface to be used as a biorecognition layer on the surface plasmon resonance spectrometer (SPR). The sensitivity, response time, and selectivity of SP-MIP are investigated by three similar analogous molecules (L-Boc-Tryptophan, L-Boc-Tyrosine, and L-Boc-Phenylalanine) and the imprinted particle surface showed excellent relative selectivity toward L-Boc-Phenylalanine (L-BFA) ($k = 61$), while the sensitivity is recorded as limit of detection = 1.72×10^{-4} M.

element of a biosensor is the biological receptor that allows selective detection of target molecules at defined concentration levels by a specific application. Receptors can have various molecular structures, including enzymes,^[1] DNA,^[2] aptamers,^[3] cells,^[4] as well as protein-based and signal-processing components.^[5] Synthetic receptors are robust chemicals that can bind target molecules at a rate comparable to that of biological receptors. Although natural receptors are difficult and expensive to isolate and purify, their shelf life is short.^[6] Thus, their practical utility has been limited. Indeed, there is a need for practical and low-cost disposable receptor-transducer designs. This is especially relevant for environmental and biomedical analysis. Besides, there is a trend in the biosensor field toward miniaturization. One technique that is being increasingly adopted for these purposes is molecular imprinting (MIP) technology with its high selectivity and versatility.^[7,8] MIPs have several advantages due to their resistance to extreme environments

1. Introduction

Biosensors are devices that are used to monitor and detect the presence of biological and chemical active substances through the placement of specific receptors on a transducer. The basic

such as high temperature and pressure, their adaptability to be used in various environments (acid and base), and their excellent mechanical strength.^[7,9] Molecularly imprinted polymers (MIPs) are capable of withstanding more extreme conditions than antibodies. However, when analytes containing protonable or

Z. Oluz, M. G. Yazlak, H. Duran
 Department of Materials Science & Nanotechnology Engineering
 TOBB University of Economics and Technology
 Söğütözü Cad. 43, Ankara 06560, Türkiye
 E-mail: hduran@etu.edu.tr

T. T. Kurşun
 Chemistry Department
 Gazi University
 Bandırma Cad. No:6/1, Ankara 06560, Türkiye

S. Nayab, B. Yameen
 Department of Chemistry
 School of Science and Engineering
 Lahore University of Management Sciences
 Lahore 54792, Pakistan

G. Glasser
 Max-Planck-Institute fuer Polymerforschung
 Ackermannweg 10, 55128 Mainz, Rhineland-Palatinate, Germany

H. Duran
 UNAM — National Nanotechnology Research Center and Institute of
 Materials Science and Nanotechnology
 Bilkent University
 Ankara 06800, Türkiye

 The ORCID identification number(s) for the author(s) of this article can be found under <https://doi.org/10.1002/marc.202400471>

DOI: 10.1002/marc.202400471

deprotonable groups are imprinted in neutral form in an organic medium, the selectivity performance of MIPs may deteriorate depending on the pH conditions, even though the MIP remains intact. Furthermore, MIP can be stored in a dry or wet form at room temperature for long periods of time.^[8]

Conventional molecular imprinting is prepared by confining a template molecule in a large mass of bulk polymer. This process uses a multi-component mixture of functional monomers, cross-linking agents, a solvent to act as a porogen, and a template mold molecule. After the polymerization, the thick polymeric layer is washed in a template-selective solvent, dried, and ground into a fine powder to expose a large surface area. This process usually yields particles of extremely large size (100–10 mm) and shape distribution, with highly irregular shapes. Some template molecules remain embedded in the polymer matrix and cannot be recovered. Although an elaborate grinding process is used, the templates located in the interior of bulk polymer are very difficult to extract because of highly cross-linked polymeric chains. As a result, they have low accessibility to the functional cavities required for analyte binding.^[10] In fact, only a small portion of the original MIP can be used by this method due to the loss of potential (analyte) binding sites. Besides, the cavities formed within the polymer matrix due to uncontrollable random polymerization show a heterogeneous structure with affinity tendencies ranging from low to high.^[9,11] The presence of weak attachment regions is a disadvantage for MIP implementation. The cavities are heterogeneous because of the excessive amount of functional monomers used compared to the amount of template molecules.^[12] In addition, often the template molecule is accompanied by many different components (functional monomer, porogen, cross-linking monomer, solvent, etc.). All these components are present at different concentrations, further complicating the cross-linked polymeric matrix. Therefore, optimizing the arrangement of all of these cavities at the molecular level with the same high binding affinities poses a major problem. As a solution, the size-selective chemical modification strategy has been successfully implemented by several groups.^[13] In this strategy, sacrificial reactive agents preferentially react with larger cavities. Thus, narrower-dispersed small cavities remain for analyte molecules intently. Using a similar strategy, a five-fold increase in the selectivity of an enantiomeric analyte was observed.^[14] This strategy is later named guest-directed chemical modification. To secure specific binding sites, the desired cavities are first protected, and then the remaining unwanted cavities are neutralized by a chemical reaction. This is accomplished by using a guest molecule. Guest molecules preferably go to high-affinity cavities and protect them. After the cavity homogenization process is finished, the high-affinity sites are made more accessible for target analyte molecules. Using this strategy, Umpleby et al.^[13] created a racemic MIP with an equal number of L- and D-selective binding sites. This racemic MIP was then chemically modified to preserve the L-selective binding sites, while the D-selective sites were eliminated. When the guest group that was not covalently bound was washed, MIP with a high enantio-selective property with only L-selective cavities was obtained.

Another limitation of conventional MIP processes is the limitation of the mass transfer rate of the target analyte molecule. High resistance to mass transfer seriously delays the access of target analytes to functional groups located in even deeper cavi-

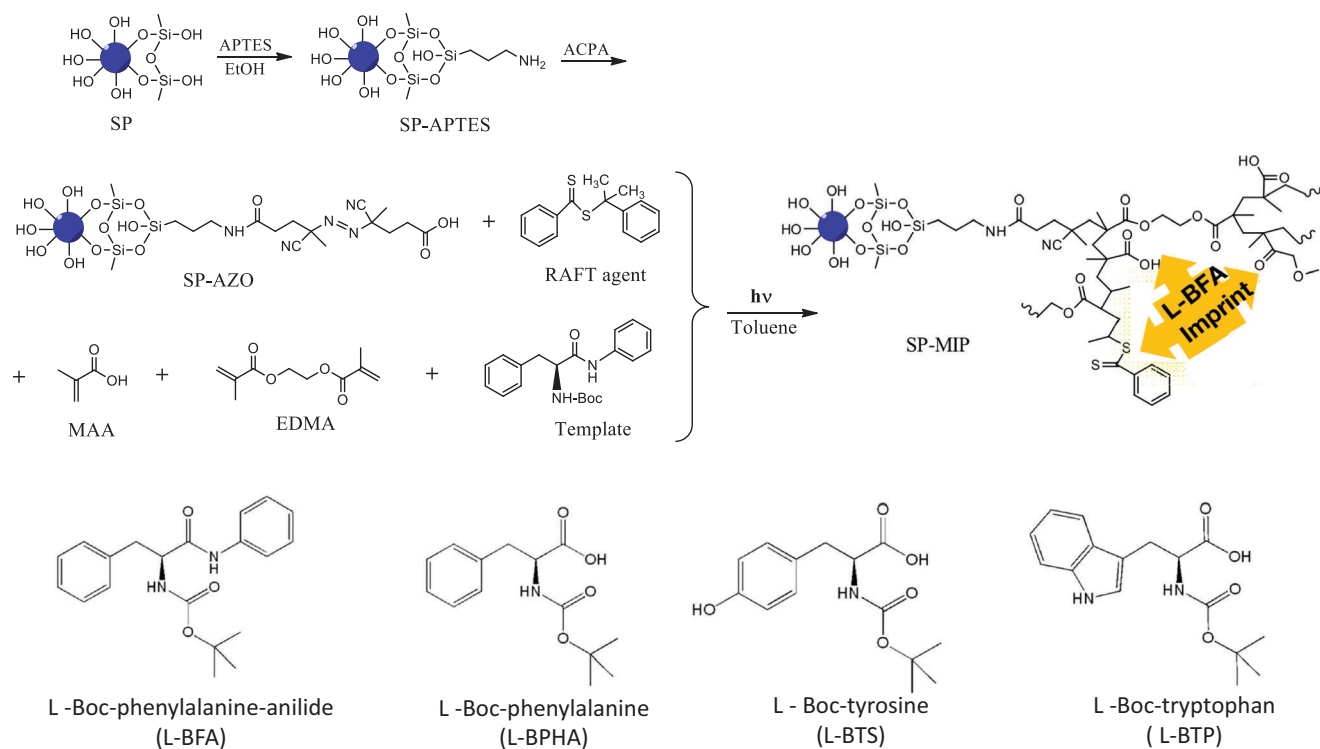
ties. As a result, binding kinetics slow down.^[7,8] Several groups have attempted to increase total porosity by adding polymeric porogens to increase access to imprinted sites and overcome diffusive limitations.^[15] However, this solution is only effective for small analyte molecules. Similarly, Tominaga et al.^[12] used specific ionic complexes attached to the surface of cross-linked polymer pores for selective recognition of the paralytic shellfish poison saxitoxin. Compared to commonly used MIPs, selectivity has increased significantly. However, various studies in recent years have shown that the surface-imprinting approach can provide a possible solution to all the issues mentioned above compared to bulk polymerization^[16–18] such as microcontact printing,^[19] surface grafting printing^[20] and core-shell nanoparticle surface printing.^[21] Shea et al.^[22–24] have clearly demonstrated that surface imprinting is much more effective than bulk imprinting. Template molecules are fixed on solid substrates to control the formation of the imprinted sites on the surface. After template removal, the selective regions are located on the surface and the target molecules gain high mobility. Thus, this approach offers good control over key parameters such as controlling the position of template molecules, better mass transfer, easy access for analyte molecules, and controlling the orientation of binding functional groups. Imprinting on nanostructure surfaces is also promising due to a high surface-to-volume ratio. The template molecules are placed on the outermost surface of the nanostructures with high precision. As a result, the distribution of effective binding sites on imprinted nanoparticles is greatly improved.^[25] Apart from further expanding the surface area of affinity sites and increasing their accessibility, nanostructured MIP films provide easy control of surface properties, such as wettability.^[12] Another advantage is that molecularly printed nanomaterials can be mounted directly on the sensor transducers. MIP-based transducers are used for electrochemical,^[26] optical waveguide,^[27,28] surface-plasmon resonance spectroscopy (SPR),^[29] and quartz crystal microbalance (QCM)^[30] sensors. Fortunately, these sensors often use metals (due to their good electrical and thermal conductivity) as transducers, which helps to easily adapt developed MIP protocols to all.

In this study, we produced surface-imprinted silica nanoparticles (SP-MIPs) on gold-coated high-refractive-index glass surfaces in the presence of a template molecule (L-Boc-phenylalanine anilide, L-BFA). SP-MIPs were fabricated via reversible addition-fragmentation chain transfer polymerization (RAFT). The chemical and surface topography properties of SP-MIP were examined by X-ray photoelectron spectroscopy (XPS) and scanning electron microscope (SEM). The sensitivity, response time, and selectivity of SP-MIP were investigated by three similar analogous molecules (L-Boc-Tryptophan, L-Boc-Tyrosine, and L-Boc-Phenylalanine) by surface plasmon resonance spectroscopy.

2. Results and Discussion

2.1. Silica Nanoparticle (SP) Synthesis and Gold Surface Modification

Silica nanoparticles (SP) were synthesized using the Stöber method and are spherical with a smooth surface. A linker molecule (APTES) covered the pristine SP followed by a reaction



Scheme 1. Schematic representation of the imprinting of L-Boc-phenylalanine anilide (L-BFA) on copolymer films from silica supports controlled by RAFT polymerization and the chemical structure of the template (L-BFA) and structurally similar analog molecules.

with an azo initiator to prepare for further surface functionalization. Methacrylic acid (MAA) and ethylene glycol dimethacrylate (EGDMA) monomers were polymerized in the presence of RAFT agent and L-BFA via UV-assisted RAFT polymerization. The overall process is represented in **Scheme 1**.

The functionalization steps were followed by XPS chemical analysis (**Figure 1**). The signal for the C1s orbital of SP-APTES consists of three peaks corresponding to C–C, C–N, and C–H bonds at 287.83, 285.2, and 284.61 eV, respectively. The presence of N1s orbital signal at 399.25 and 401.14 eV in the XPS survey scan of SP-APTES implies the amine functionalization. The immobilization of the azo initiator layer is validated by the C1s signal assigned to C=N at 288.67 eV and the N1s signal at 400.25 eV which is assigned to the cyanate group in the initiator structure. The XPS spectrum of S 2p_{3/2} reveals an asymmetric band that can be fitted by two peaks at 163.0 and 164.5 eV (**Figure 1e**). While the strong peak at 163.0 eV is assigned to S–Au bond, the shorter peak at 164.5 eV can be attributed to free sulfur atoms.^[31] An important gain of this sulfur is that it helps to bind the nanoparticles to the gold surface. The driving force for anchoring thiols on gold surfaces is the formation of a thermally stable Au–S bond.^[32]

Thermogravimetric analysis was performed to validate the surface modification (**Figure S1**, Supporting Information). Pristine SP showed a weight loss of up to 150 °C due to adsorbed water and impurities on the surface, and a total weight loss of 10.26% exhibited at temperatures of up to 900 °C, which was attributed to the removal of silanol groups. In the case of SP-APTES and SP-AZO, weight loss was 12.08% and 12.14%, respectively, which was attributed to modified organic layer decomposition. By graft-

ing the imprinted copolymer layer onto the surface of the silica nanoparticles, the weight loss increased to 13.28% for SP-MIP.

The specific surface area of the SP was obtained by BET analysis as 69.07 m² g⁻¹. On the other hand, the specific surface areas for all functionalized SPs were drastically decreased. The extent of L-BFA imprinting was followed by calculating the difference between the specific surface area of SP-MIP and that of non-imprinted particles, SP-NIP. SP-MIP exhibited a specific surface area of 17.20 ± 1.58 m² g⁻¹, while this value was 12.22 ± 2.77 m² g⁻¹ for SP-NIP (**Table S1**, Supporting Information). This difference confirms the presence of L-BFA-imprinted molecular sites since SP-MIP exhibited a larger surface area, a factor of 1.42 compared to that of SP-NIP, only if both NPs are assumed to have the same film thickness.

The SEM investigation revealed that the pristine and surface-modified SPs are spherical with an average diameter of 114 ± 10 nm (**Figure 2a–d**). APTES and imprint layers are uniformly distributed around SPs, and bridging organic layers are discernible, especially for SPs coated with APTES and imprinted later (**Figure 2b,c**). **Figure 2d** shows the transformed SP-MIP on gold substrates. Although there is no full coverage on the surface, SP-MIPs homogeneously cover the gold surface.

The size and size distribution of SPs were analyzed using DLS and Zeta potential measurements. The hydrodynamic diameter of the pristine SP was roughly 117 ± 2 nm. Upon modification with APTES, the particle size and hydrodynamic diameter slightly increased to 166 ± 1 nm. Meanwhile, the hydrodynamic diameter of SP-NIP was 267 ± 39 nm and SP-MIP was ≈675 ± 89 nm (**Figure S2** and **Table S1**, Supporting Information).

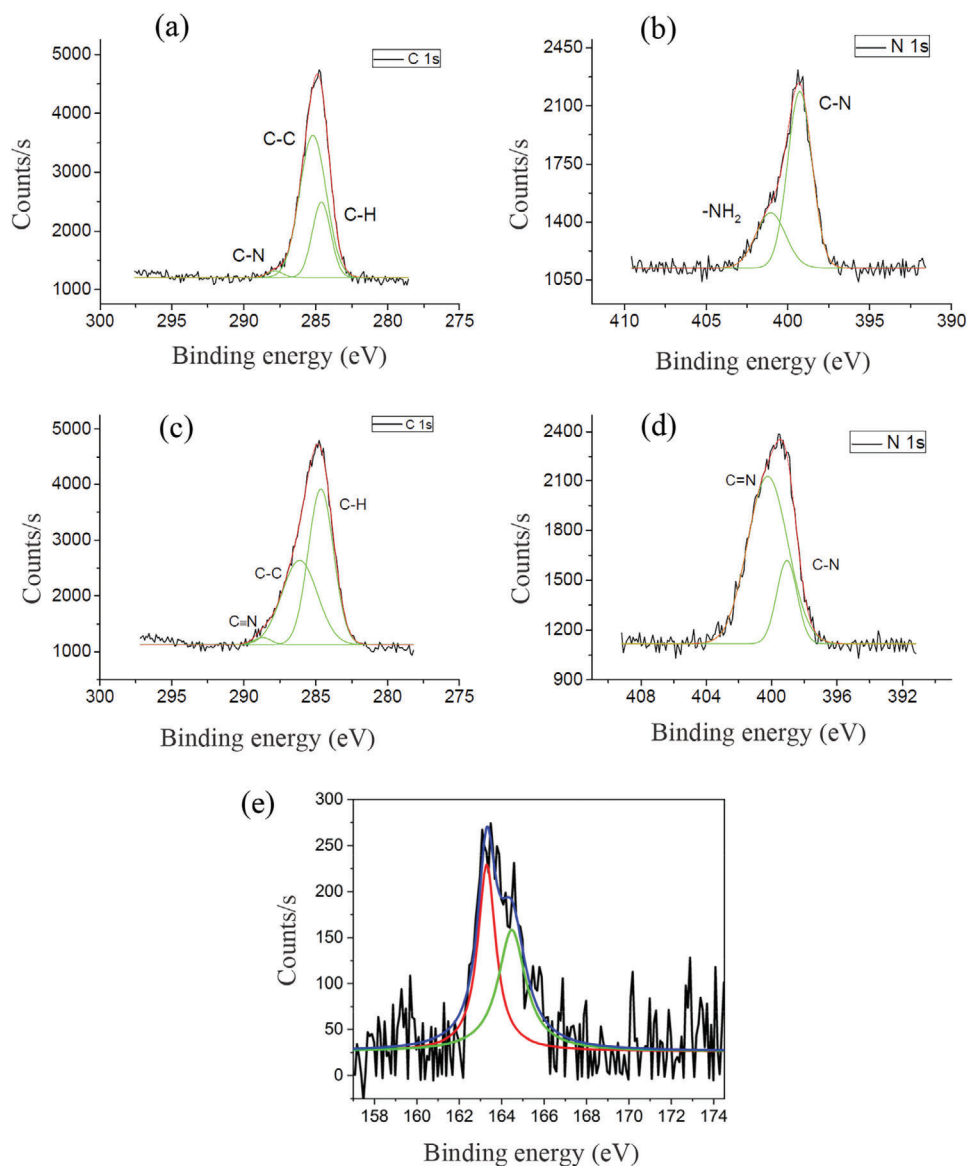


Figure 1. XPS high-resolution a,b) C 1s, N 1s scans of SP-APTES, c,d) SP-Azo, and e) S 2p scan of SP-MIP.

Based on these results, it is evident that SP-MIP forms larger clusters. Besides, The increase in the number of organic layers on the SP surface also expanded the size distribution.

2.2. SP-MIP Affinity and Selectivity Tests

In the copolymerization of MAA and EGDMA, the monomers are named functional and crosslinkers, respectively. The molar ratio of these two monomers in the polymerization solution determines the crosslinking density and stability of the cavities in the structure of the polymer produced. If the polymer layer is swelling, the geometry of the cavities is altered, and the sensor performance is adversely affected. Thus, the molar ratio of the functional monomer and the cross-linking monomer needs to be well adjusted. The molar ratio is used as 1:5 and 1:10 for

crosslinker: functional monomer. The optimization of molar ratios was analyzed based on SPR measurements.^[33–35] Thus, before binding tests of the template and analog molecules, swelling tests were conducted on both ratios. SP-MIPs attached to the gold surface served as transducers for bioaffinity support evanescent waves excited by using the Kretschmann configuration of the attenuated total reflection method. The sensor surface was kept in MeOH/H₂O 1:1 (v/v) and followed by SPR scans for a maximum of 48 h. Figure 4a,b shows the measured angular reflectivity spectra of SP-MIP with 1:5 and 1:10 EGDMA:MAA functional monomer ratios, respectively. A change in the resonant coupling angle ($\Delta\theta$) of 0.20° was observed for a 1:5 crosslinker: monomer ratio in 24 h (Figure S4a, Supporting Information). This indicated a slight swelling of the SP-MIP. When the ratio of the monomer to the crosslinker increases to 1:10, the total shift of the resonance angle is almost indiscernible (Figure S4b, Supporting Informa-

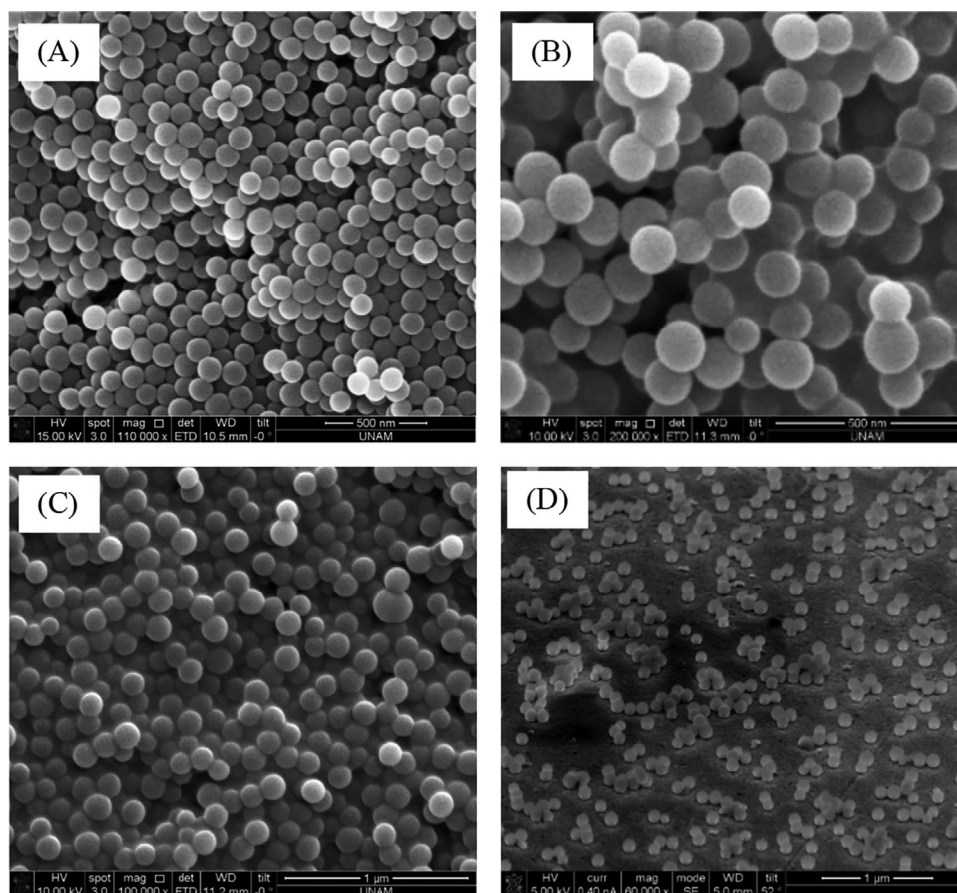


Figure 2. SEM images of a) pristine SP, b) SP-APTES, c) SP-MIP, and d) SP-MIPs on a gold substrate.

tion). It was decided to continue with the 1:10 ratio to prevent interference of the polymer layer swelling with the sensor's response to the analyte molecule.

To follow the affinity performance and selectivity of imprinted cavities on the sensor surface, the shift in resonance angle ($\delta\theta_r$) was measured for SP-MIP and control (SP-NIP) samples for the L-BFA imprint molecule, as well as three structurally similar control molecules. The L-BFA concentration ranged from 0.2 to 2×10^{-3} M. First, the resonant angle change due to the flow of a MeOH/H₂O 1:1 (v/v) solvent mixture ($\delta\theta_s$) was measured as a reference and the sensor output was determined as the ratio ($\delta\theta_r / \delta\theta_s$). The accumulation of L-BFA and analog molecules in SP-MIP and SP-NIP was estimated from the changes of the resonance coupling angle $\delta\theta_r$ changes. This analysis shows that the presence of L-BFA in the concentration of 2×10^{-3} M concentration leads to $\approx 3^\circ$ shift of $\delta\theta_r$ (Figure 3a). The resonance angle change was measured for the analog molecules as 0.39 for L-BTP, 0.07 for L-BTS, and 0.05 for L-BPHA. However, almost no change was detected for SP-NIP (Figure S5, Supporting Information). Moreover, measured resonance angle scans reveal that the angle shift increases with L-BFA concentration. Compared to SP-MIP and SP-NIP, SPR angular scan analysis confirms L-BFA accumulated in SP-MIP (Figure 3a,b). The calibration curve obtained presented in Figure 3c reveals that the limit of detection (LOD) is 1.72×10^{-4} M. This value is two orders of magnitude

higher than the embedded hydrogel waveguides with molecularly imprinted polymer nanoparticles.^[28]

To evaluate the sensitivity with which the refractive index changes (δn) in the immediate environment of SP-MIP, we performed solvent exchange experiments using ethanol, deionized water, and methanol at room temperature (24 °C) as model liquids with very close n and ϵ values (Figure S6, Supporting Information). An increase in the refractive index of the SP-MIP layer due to immersion of three different solvents was followed by a shift in the critical angle $\delta\theta_c$ and a change in the corresponding effective refractive index (δn_s) which leads to a change in the resonant coupling angle $\delta\theta_r$. Changes of $\delta\theta_r = 0.20$ and 0.40° were observed with successive flows of water and methanol that correspond to the effective refractive indices of $n = 1.334$ ($\epsilon = 1.781$) and 1.331 ($n = 1.325$, $\epsilon = 1.756$) as determined from changes in θ_c . The positions of the experimentally obtained reflectivity minima were in good agreement with Fresnel calculations with the effective refractive indices as the only adjustable variable. The achievable merit figure (FOM) was calculated from the sensitivity of the refractive index (slope) of $S = \delta\theta_r / \delta n_s = 66.67^\circ$ per refractive index unit (RIU) for SP-MIP and from the full width at half the minimum (fwhm) of the considered reflectivity peak (Γ). $FOM = (\delta\theta_r / \delta n_s) / \Gamma$ was calculated as ≈ 30 (RIU⁻¹) at $\lambda = 632.8$ nm. This value is in the range with previously reported porous silica film-based SPR sensors,^[36]

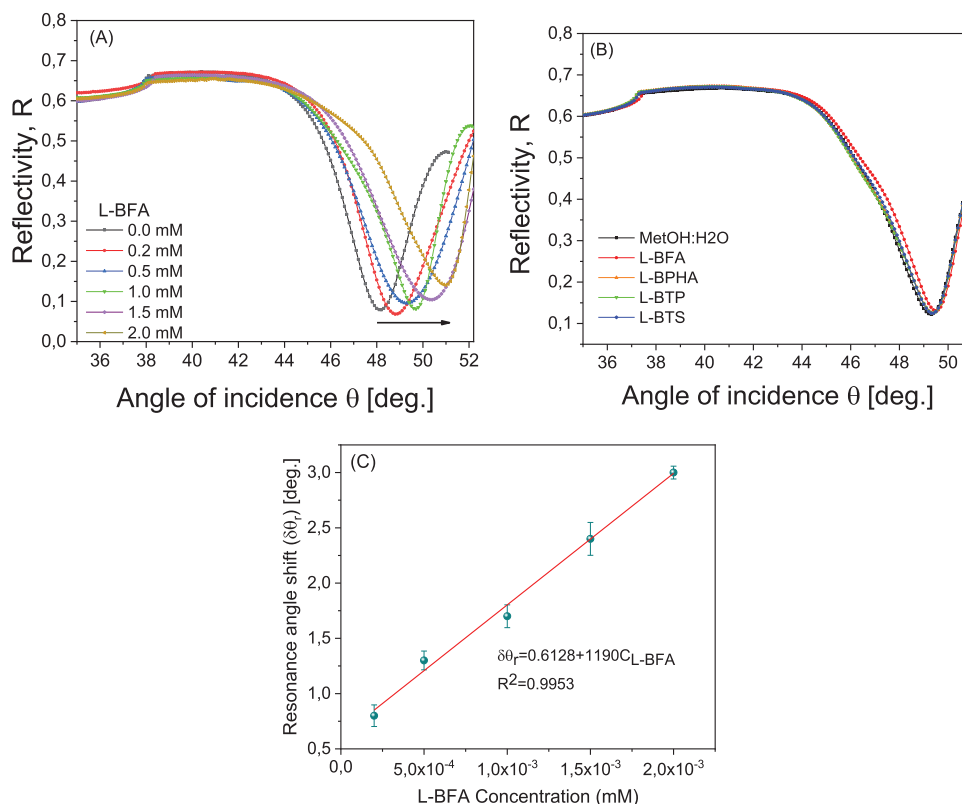


Figure 3. SPR angular reflectivity spectra of a) SP-MIP with L-BFA concentration ranging from 0 to 2 mM, respectively, b) angular reflectivity spectra of 1 mM L-BFA, L-BPHA, L-BTP, and L-BTS, and c) The calibration curve showing the linear relationship between the resonance angle shift and L-BFA concentration.

however, slightly lower than optical waveguide spectroscopy.^[28,37] For example, Sharma et al.^[28] reported FOM of 52 RIU^{-1} for molecularly imprinted polymer nanoparticles embedded in a poly(N-isopropylacrylamide)-based hydrogel. This is understandable since the resonance dip widths of waveguide modes are much narrower than SPR. In order to obtain sharper resonance peaks, it is necessary to obtain leaky optical waveguide modes. This is possible by increasing the thickness (or number of layers) of the silica NPs. Using the Maxwell–Garnett (MG) theory, SPR and waveguide modes were calculated by increasing the film thicknesses (or number of silica NPs layers) for 100 nm diameter SPs. The curves in **Figure 4** show the simulated reflectivity as a function of the angle of incident for TM mode. As the number of SP layers increases, the T_{m0} (SPR resonance peak) shifts slightly due to the change in $\epsilon^{\text{effective}}$ with the void fraction between SPs (refer to Supporting Information for Maxwell–Garnett calculations). However, the peak becomes narrower with increasing layer thickness. Beyond a layer thickness of 300 nm, the first waveguide peaks start to appear. These peaks are much narrower, and the responds to the change in the medium's refractive index significantly (e.g., for $\delta n = 0,0024$ between 500 and 400 nm thick SP, $\delta\theta_{T_{m0}} = 0.403^\circ$, $\delta\theta_{T_{m1}} = 6.031^\circ$ and $S_{M0} = 170.50^\circ$, $S_{M1} = 2551^\circ$, respectively). Based on this simulation, FOM was calculated to be $43.175 \text{ (RIU}^{-1}\text{)}$ and $1300 \text{ (RIU}^{-1}\text{)}$, respectively. These calculations clearly show that our experimentally observed sensitivity for SPR approaches the theoretical limit. To increase

sensitivity further, it is essential to use multilayer SP to obtain narrower optical waveguides.

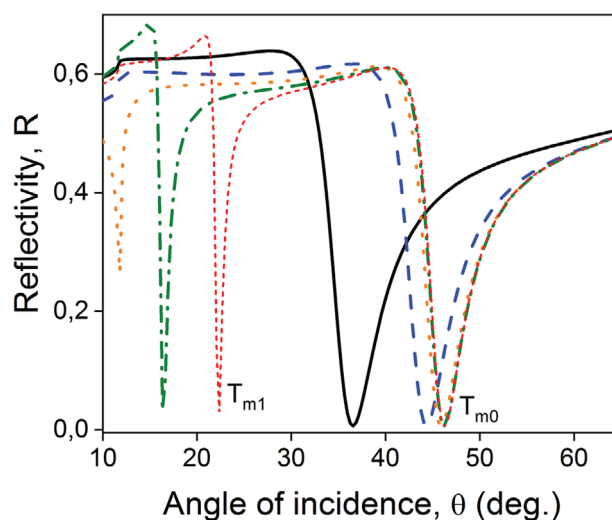


Figure 4. Simulated reflectivity versus incident angle curves for SPs ($D = 100 \text{ nm}$) in MeOH/ H_2O 1:1 (v/v) mixture with the layer thickness of 100 nm (solid black), 200 nm (blue dash), 300 nm (orange dots), 400 nm (green dash-dot) and 500 nm (red short-dash), respectively, at the wavelength of 632.8 nm.

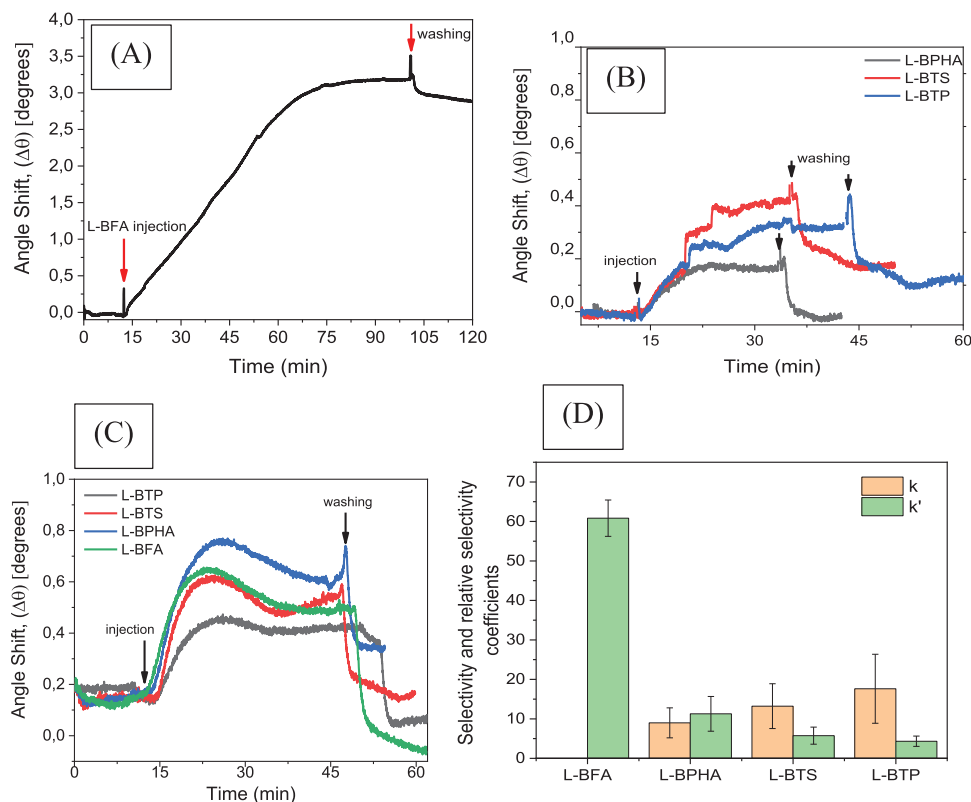


Figure 5. Kinetics of affinity binding of SP-MIP a) 2 mM L-BFA, b) 2 mM analog molecules (L-BPHA, L-BTS, and L-BTP) c) control SP-NIP, d) selectivity and relative selectivity comparison among L-BFA, L-BPHA, L-BTS, and L-BTP, respectively.

For the kinetic analysis, $\delta\theta_t$ variations due to the change in analyte concentration were followed over time. A baseline was established using a MeOH / H₂O 1:1 (v/v) solution before flowing L-BFA or analog molecules. Subsequently, the analyte molecule with various concentrations (0–2 mM) was injected into the flow cell. When the surface was saturated with the analyte, samples were washed to remove the physisorbed molecules. The surface reached saturation \approx 60 min after injection of 2 mM L-BFA (Figure 5a). For analog molecules, the saturation point was reached much earlier (\approx 15 min) (Figure 5b). Furthermore, the interaction of a structurally very similar molecule (L-BPHA) at the same concentration resulted in one order of magnitude lower response on the SP-MIP surface than the target analyte L-BFA. The control SP-NIP sensor was analyzed to determine whether there was non-selective binding (Figure 5c). The baseline was achieved in the first 15 min, and the adhesion was observed within the first 3 min after the flow of molecules. The surface reached saturation in \approx 10 min. After washing with MeOH / H₂O, it was found that the surface returned to its initial point for most analytes. The molecules were physisorbed to the surface and could be removed from the surface in 2 min.

The selectivity of the developed SP-MIP sensor for the detection of L-BFA was tested by comparing the response with SP-NIP to target L-BFA and other structurally similar analytes of L-BPHA, L-BTP and L-BTS (Figure 5d). The selectivity coefficient (k) and relative selectivity coefficients (k') were calculated for

both SP-MIP and SP-NIP sensors using Equations (1) and (2) as:^[29,38]

$$k = \delta\theta_{-L-BFA} / \delta\theta_{analog} \quad (1)$$

$$k' = k_{SP-MIP} / k_{SP-NIP} \quad (2)$$

The highest relative selectivity (k') was observed for L-BFA, followed by L-BPHA. These two molecules are very similar in chemical structure, with the only difference being the presence of a carboxylic group instead of the anilide group for L-BFA. However, the selectivity (k) ratio between L-BFA and L-BPHA is still high, indicating the specific affinity of the cavities in SP-MIPs for the target analyte. The molecule L-BTP, which is further from L-BFA in terms of chemical structure, had the highest selectivity coefficient compared to other analog molecules. This is because the additional steric bulk of the side chain indolyl group might limit the access of L-BTP to the binding site prepared by L-BFA. As a result, the selectivity coefficient (k) systematically increased from the molecule that is most similar in structure (L-BPHA) to the template L-BFA, to the molecule that is furthest away from it (L-BTP).

Over the last four decades, L-BFA and analog molecules have been used as model materials for testing the efficiency of molecularly imprinted polymers for the enantioseparation of D,L-aromatic amino acids. Therefore, there are many studies on the selectivity of the target analyte and similar analog molecules used

Table 1. Performance evaluation of newly designed SP-MIP with the various support materials for the L-BFA target analyte as a function of selectivity, limit of detection, and figure of merit values.

Analyte/test molecules	Imprinting method/support material/detection technique	Selectivity, k and k'	LOD [M]	FOM [RIU ⁻¹]	Reference
L-BFA/L-BTP, L-BPA, and L-BTS	RAFT/ polymer nanoparticle/ optical waveguide spectroscopy	k' = 14 k = 2	2 × 10 ⁻⁶	52	[28]
L-BFA and D-BFA	RAFT/mesoporous silica (D = 10 μm)/HPLC	k = 4	N/A	N/A	[33]
L-BFA/L-BPHA, L-BTP, L-Boc-Tyrosinamide and L-Boc-Leucineamide	mini-emulsion polym./ polymer nanospheres/reflectometric interference spectroscopy (RIFS).	k' = 3	40 × 10 ⁻⁶	N/A	[39]
L-PHA and D-PHA	Surface-initiated polym./ silica (D = 10 μm)/ capillary electrochromatography (CEC)	k = 3.35	N/A	N/A	[40]
L-BPHA/ tyrosine, pylalanine, leucine, threonine, phenylglycine.	Bulk polym. particles (1-15 μm)/Capillary Gel Electrophor.	k = 1.45	N/A	N/A	[41]
L-BPH and L-BFA/ D,L-phenylglycine, D,L-tyrosine and D,L-3-(3,4-dihydroxyphenyl) alanine.	UV or thermally curated Bulk Polym./HPLC and CEC	k = 1.5	N/A	N/A	[42, 43]
L-BFA/L-BTP, L-BPA, and L-BTS	miniemulsion polym./ microgels/ Isotherm.titration calorim.	k' = 42 k = 4	N/A	N/A	[44]
L-BFA, L-BPHA	Miniemulsion polym./polym. nanospheres/HPLC and UV-vis-spectr.	k' = 1.93	N/A	N/A	(Lehmann et al., 2004)
L-BFA, L-BTP, L-BPA, and L-BTS	RAFT/ silica nanoparticle/SPR	k' = 61 k = 17	1.72 × 10 ⁻⁴	30	This study

in the study (Table 1). When we compare it with these data, it is seen that the highest selectivity ($k = 17$ for B-TRP) and relative selectivity ($k' = 61$) have been achieved with the surface imprinting of the L-BFA molecule on a silica nanoparticle with RAFT polymerization.

3. Conclusion

A surface imprinted silica nanoparticle containing L-BFA target imprint cavities as a highly selective transducer surface for optical detection is reported. The imprinted surface was supported by ≈100 nm diameter silica nanoparticles synthesized by the Stöber method. RAFT polymerization was applied to control the imprinted layer cross-linking and thickness, which is an important parameter in providing easily accessible binding sites for the analyte molecule. The SPR spectroscopy of imprinted nanoparticles supported an accurate readout for the refractive index variations resulting from the imprinted sites and the interaction of analyte molecules. A low molecular weight L-BPA analyte can be detected with an LOD of 1.72×10^{-4} M. This value is one to two orders of magnitude lower than previously reported studies. One of the reasons for this may be that the width of the SPR resonant peak is much wider than that of the optical waveguides in those studies. However, our design still needs to be improved in this regard. In our future study, we plan to obtain the waveguide by increasing the thickness of the SP-MIP layered. Subtle changes in the effective refractive index of the SP-MIP were detected at high sensitivity using ethanol, deionized water, and methanol at room tem-

perature. The sensing figure of merit thus achieved amounted to 30 RIU⁻¹. However, the greatest success of SP-MIP has been observed in the selectivity performance between the target analyte and the analog molecules. The highest relative selectivity and selectivity were recorded at 61 and 17, respectively, and are therefore higher than that of other sensors based on angular modulation. We believe that this transducer design would be an advancement for MIP-based SPR sensors.

4. Experimental Section

Materials: Tetraethyl orthosilicate (TEOS, 99%), (3-aminopropyl) triethoxysilane (APTES), 4,4'-azobis (4-cyanopentanoic acid) (ACPA), EGDMA, MAA, N,N'-dicyclohexylcarbodiimide (DCC), 1-hydroxybenzotriazole hydrate (HOBt), L magnesium sulfate (MgSO₄), sodium bicarbonate (NaHCO₃), aqueous ammonia (NH₃, 35%), concentrated hydrochloric acid (36.6-38%), sodium methoxide, sulfur, diethyl ether, α-methyl styrene, dichloroethane, ethyl acetate, ethanol, and hexane were used as received and obtained from Sigma-Aldrich (Germany). Template molecules: L-Boc-phenylalanine, L-Boc-tyrosine, and L-Boc-tryptophan were purchased from Merck (Darmstadt, Germany). Solvents, toluene (99%), methanol, dichloromethane (DCM), and dimethyl formamide (DMF) were also obtained from Merck (Germany) and stored in a molecular sieve (3 Å) overnight before use. Aniline was obtained from Sigma-Aldrich (Germany) and used as a freshly distilled. The template, L-Boc-phenylalanine anilide (L-BFA) and 2-phenylprop-2-yl-dithiobenzoate were synthesized following previously described procedures.^[45,33] High-refractive-index glass substrates (LSFN9) were purchased from Hellma Optics, Germany. The chemical structure of L-Boc-phenylalanine anilide (L-BFA),

L-Boc-phenylalanine (L-BPHA), L-Boc-tyrosine (L-BTS), and L-Boc-tryptophan (L-BTB) is given in Scheme 1.

Synthesis of Silica Nanoparticles (SP): SPs were prepared according to a previously reported method.^[46] Briefly, 7 mmol of TEOS was added dropwise to a solution containing 20 mmol of aqueous ammonia in 330 mL of methanol. The mixture was stirred at 60 °C for 5 h, then separated by centrifugation at 4000 rpm for 20 min, followed by washing three times with ethanol and dried in an oven at 60 °C.

Synthesis of Linker-Coated Silica (SP-APTES): 5.5 mL of (3-aminopropyl) triethoxysilane (APTES) was added to the previously synthesized bare SP dissolved in 330 mL of methanol and stirred overnight at room temperature. The APTES coated particles were separated by centrifugation at 4000 rpm for 20 min followed by washing three times with ethanol and drying in an oven at 60 °C.

Synthesis of Initiator-Modified Silica (SP-AZO): The surface of SP-APTES was modified with 4,4'-azobis (4-cyanopentanoic acid) which was used as azo initiator. The 2.8 mmol initiator was dissolved in 20 mL of dry DCM containing 260 µL dry TEA in an N₂ atmosphere. 0.6 g of degassed SP-APTES particles were added to the medium and stirred 2.5 h at room temperature. SP-AZO was washed twice with both DCM and ethanol and dried overnight before use.

Synthesis of SP-MIP with L-BFA Imprint Molecule Via RAFT Polymerization: 1 g of SP-AZO, L-BFA (1 mmol), RAFT agent (0.74 mmol), MAA (8 mmol) and EGDMA (80 mmol) were dissolved in 11 mL of dry toluene. In order to control the crosslinking density, two different molar ratios of the functional monomer and the cross-linking monomer were used as 1:5 and 1:10 for EGDMA:MAA. After the polymerization solution was purged with N₂, the reaction was started with UV irradiation (254 nm) and allowed to continue for 90 and 120 min. Non-imprinted copolymer-coated nanoparticles were prepared in the absence of L-BFA (SP-NIP).

Synthesis of RAFT Agent [2-phenylprop-2-yl dithiobenzoate (cumyl dithiobenzoate, CDB)]: 0.50 mol of sodium methoxide, and 0.50 mol of elemental sulfur were dissolved in 160 mL of dry methanol and 0.25 mol of benzyl chloride was added to the medium dropwise in 60 min at room temperature. The reaction mixture was kept at 70 °C for 18 h, then cooled to 5 °C in an ice bath. The precipitate was filtrated and methanol evaporated. The solid residue was dissolved in 100 mL of water and washed with diethyl ether three times. 1.0 M HCl (250 mL) and diethyl ether were added, and dithiobenzoic acid was transferred to the ether phase. After washing the ether phase three times with water, 1.0 M NaOH (250 mL) was added to the medium to deprotonate dithiobenzoic acid and extract dithiobenzoate (DTB) from the water phase. The water phase containing the product was washed three times with diethyl ether, and then 1.0 M HCl (250 mL) was added to extract DTB from the ether phase and washed three times with water. The ether layer was dried with MgSO₄ and diethyl ether was removed under vacuum. The final product was in oil form. DTB (72.0 mmol) and α -methyl styrene (88.0 mmol) were dissolved in dichloromethane (40 mL), then the solution was purged with nitrogen for 5 min and stirred for 6 h at 70 °C. After the solvent was evaporated, CDB as dark purple oil was purified by column chromatography (n-hexane). ¹H¹ NMR for CDB (400 MHz, CDCl₃): δ 7.86 (d, 2H), 7.20–7.60 (m, 8H), 2.05 (s, 6H).

Synthesis of Template Molecule L-BOC-Phenylalanine Anilide (L-BFA): 0.05 mol of freshly distilled aniline was added to the solution containing 0.06 mol of L-Boc-phenylalanine, 0.06 mol of HOBt, and 0.08 mol of DCC in 150 mL of dry DMF. After a few hours of mixing, the mixture was filtered, dried with MgSO₄, and dried at the rotational evaporator. The solid residue was dissolved in DCM and then washed with 1 M NaHCO₃, 0.5 M HCl, and water, respectively. After DCM evaporation, the residue was purified by column chromatography (2.5:1 hexane: ethyl acetate). ¹H¹ NMR for L-BPHA (400 MHz, CDCl₃): δ 1.42 (s, 9H), 3.14 (d, 2H), 4.47 (s, 1H), 5.18 (s, 1H), 7.26–7.37 (m, 3H), 7.77 (s, 1H). ¹H¹ NMR for L-BFA (400 MHz, CDCl₃): δ 1.95 (s, 9H), 2.85 (m, 1H), 3.67 (m, 1H), 7.03 (m, 2H), 7.24 (m, 3H), 7.32–7.29 (m, 2H), and 7.62 (m, 3H).

Placing SP-MIP and SP-NIP on the Gold Surface: 2 nm thick chromium and 47 nm thick gold layers were coated on LSFN9 glass substrates by vacuum thermal evaporation after cleaning the high refractive index glass ($n = 1.8$) with Hellmanex III. Various techniques such as drop casting, spin coating, and dip coating were employed to stabilize nanoparticles on

top of the gold surface. However, dip coating was preferred because it can coat nanoparticles uniformly on the substrate. Solutions containing SP MIP, with concentrations ranging from 1 to 10 mg mL⁻¹, were vortexed for 1 min, sonicated for 20 min, and then the gold substrate was placed in the solution horizontally and left overnight. Then, the SP MIP deposited gold substrates were washed three times with pure water and ethanol, respectively, and subjected to heat treatment at 40 °C for 5 h for fixation of nanoparticles. The procedure was repeated four to eight times, depending on the concentration of SP MIP. SEM images of the gold substrate showed that the most efficient coating was achieved with SP MIP at a concentration of 7.5 mg mL⁻¹, resulting in a uniform and stable layer.

Characterization: Scanning electron microscopic (SEM) images were obtained by using a FEI Quanta 200 FEG instrument with an accelerating voltage of 5 kV. X-ray photoelectron spectroscopy (XPS) measurements were carried out using Thermo Scientific K-Alpha. The Mg K α (1253.6 eV) X-ray source was operated at 300 W. A pass energy of 117.40 eV was used for the survey scans. The spectra were recorded using a 60° take-off angle relative to the surface normal. UV–vis absorption spectra were recorded using a PerkinElmer Lambda 25 UV/Vis spectrophotometer. Surface analyses were performed using the Nova 1000e BET Pore Analyzer after degassing the samples overnight before measurement. Thermogravimetric analysis (TGA) was performed with a TGA Q50 V6.2 Build 187 from room temperature to 900 °C at a heating rate of 10 °C min⁻¹ under a nitrogen flow (40 mL min⁻¹). NMR was used to verify the chemical structure and to provide impurity control of the L-BFA and RAFT agents. The ¹H-NMR spectra of the solutes in the CDCl₃ environment were obtained using a Bruker AVANCE III 400 MHz liquid NMR Spectrometer (\approx 9 Tesla). The Nicolet 6700 FT-IR spectrometer was used to obtain FT-IR spectra. The hydrodynamic radius and polydispersities of SPs in distilled water (pH 7) were measured using Malvern Zeta Nano ZS. The study was carried out at 25 °C at a wavelength of 633 nm with a 5 mW He–Ne laser source. Measurements were taken every 5 min for the first hour to calculate the average hydrodynamic radius values of SPs. Zeta potential measurements were also taken to observe the stability of SPs.

The bioaffinity performance of L-BFA and other analogous molecules was followed by surface plasmon resonance spectroscopy (SPR), with Kretschmann configuration.^[47] A monochromatic TM polarized laser beam from the He–Ne laser ($\lambda = 632.8$ nm) was coupled to a 90° LASFN9 optical prism and reflected from the base of the prism. The prepared sensor chip was optically matched to the prism by index-matching liquid. The transducer surface consists of 48 nm gold and 2 nm chromium layers with SP-MIP or SP-NIP on the top. The transducer surface was then attached to a flow cell (volume = 1 mL) of which the input and output ports were connected to a rubber tube peristaltic pump. The liquid samples were flowed through the surface with a flow rate of 50 µL min⁻¹. The combination of prism and flow cell was placed on a rotation stage with an angle resolution of $\theta = 0.005^\circ$, and surface plasmon excitations were followed by angular reflectivity spectra measured $R(\theta)$ using a photodiode detector and a lock-in amplifier. The angular reflectivity $R(\theta)$ spectra were recorded by changing the angle of incidence of light. With the help of this setup, surface plasmons occurred when the excitation laser and surface plasmon were phase-matched along the metal surface. The angle of incidence was fixed at the angle referring to the medium reflectivity of the spectrum for time-dependent kinetic measurements. The optical setup was controlled by Wasplas software, which was developed at Max–Planck Institute for Polymer Research, Germany.

Supporting Information

Supporting Information is available from the Wiley Online Library or from the author.

Acknowledgements

H. D. gratefully acknowledges the Turkish Scientific and Technological Research Council (TUBITAK) for the financial support of Project No. 112M804.

Conflict of Interest

The authors declare no conflict of interest.

Author Contributions

Z.O. performed data curation and formal analysis, developed methodology, and wrote the original draft. G.Y. developed a methodology and performed data curation, formal analysis, and validation. T.T.K. performed data curation, formal analysis, and investigation. S.N. performed data curation, formal analysis, and developed methodology, G.G. performed data curation, and formal analysis. B.Y. performed conceptualization and acquired resources. H.D. performed conceptualization, supervision, investigation, and project administration, acquired resources and Funds, and wrote, reviewed, and edited the final draft.

Data Availability Statement

The data that support the findings of this study are available from the corresponding author upon reasonable request.

Keywords

L-Boc-phenylalanine, molecularly imprinted polymers, optical biosensor, RAFT polymerization, silica nanoparticle, surface imprinting, surface plasmon resonance

Received: June 19, 2024

Revised: July 24, 2024

Published online: August 26, 2024

- [1] M. Maiga, I. Yazgan, V. M. K. D. O. Demirkol, O. A. Sadik, S. Timur, *Sensors Actuators B Chem* **2018**, 256, 71.
- [2] L. Li, C. Niu, T. Li, Y. Wan, Y. Zhou, H. Wang, R. Yuan, P. Liao, *Biosens. Bioelectron.* **2018**, 101, 206.
- [3] G. Wang, X. Su, Q. Xu, G. Xu, J. Lin, X. Luo, *Biosens. Bioelectron.* **2018**, 101, 129.
- [4] L. T. Bereza-Malcolm, G. Mann, A. E. Franks, *ACS Synth. Biol.* **2015**, 4, 535.
- [5] J. Manhas, H. I. Edelstein, J. N. Leonard, L. Morsut, *Nat. Chem. Biol.* **2022**, 18, 244.
- [6] D. R. Kryscio, N. A. Peppas, *Acta Biomater.* **2012**, 8, 461.
- [7] K. Haupt, K. Mosbach, *Chem. Rev.* **2000**, 100, 2495.
- [8] G. E. M. Tovar, I. Kräuter, C. Gruber, *Colloid Chemistry II*, (Ed: M. Antonietti), Springer, Berlin, Heidelberg **2003**, Ch. 5 pp 125–144.
- [9] G. Guan, B. Liu, Z. Wang, Z. Zhang, *Sensors* **2008**, 8, 8291.
- [10] E. Yilmaz, R. H. Schmidt, K. Mosbach, *Molecularly Imprinted Materials Science and Technology*, 1st ed., CRC Press, Boca Raton, FL, USA, **2004**, 25.
- [11] J. Erdőssy, E. Kassa, A. Farkas, V. Horváth, *Anal. Methods* **2017**, 9, 4496.
- [12] Y. Tominaga, T. Kubo, K. Kaya, K. Hosoya, *Macromolecules* **2009**, 42, 2911.
- [13] R. J. Umpleby, G. T. Rushton, R. N. Shah, A. M. Rampey, J. C. Bradshaw, J. K. Berch, K. D. Shimizu, *Macromolecules* **2001**, 34, 8446.
- [14] S. McNiven, Y. Yokobayashi, S. H. Cheong, I. Karube, *Chem. Lett.* **1997**, 26, 1297.
- [15] A. S. Belmont, S. Jaeger, D. Knopp, R. Niessner, G. Gauglitz, K. Haupt, *Biosens. Bioelectron.* **2007**, 22, 3267.
- [16] E. Mazzotta, T. Di Giulio, C. Malitesta, *Anal. Bioanal. Chem.* **2022**, 414, 5165.
- [17] C. Unger, P. A. Lieberzeit, *React. Funct. Polym.* **2021**, 161, 104855.
- [18] A. Turco, S. Corvaglia, E. Mazzotta, P. P. Pompa, C. Malitesta, *Sensors Actuators B Chem* **2018**, 255, 3374.
- [19] E. Meyer, H. G. Braun, *Macromol. Mater. Eng.* **2000**, 276, 44.
- [20] A. Sun, J. Chai, T. Xiao, X. Shi, X. Li, Q. Zhao, D. Li, J. Chen, *Sensors Actuators B Chem* **2018**, 258, 408.
- [21] X. Kong, R. Gao, X. He, L. Chen, Y. Zhang, *J. Chromatogr. A* **2012**, 1245, 8.
- [22] N. A. O'Connor, D. A. Paisner, D. Huryn, K. J. Shea, *J. Am. Chem. Soc.* **2007**, 129, 1680.
- [23] H. Nishino, C. S. Huang, K. J. Shea, *Angew. Chem. Int. Ed.* **2006**, 45, 2392.
- [24] F. W. Scheller, U. Wollenberger, A. Warsinke, F. Lisdat, *Curr. Opin. Biotechnol.* **2001**, 12, 35.
- [25] S. M. Amininasab, P. Holakoei, Z. Shami, M. Hassanzadeh, *J. Polym. Res.* **2018**, 25, 84.
- [26] S. Alexander, P. Baraneedharan, S. Balasubrahmanyam, S. Ramaprabhu, *Eur. Polym. J.* **2017**, 86, 106.
- [27] G. Wang, C. Wang, S. Sun, *Sensors Actuators B Chem* **2018**, 255, 3400.
- [28] N. Sharma, C. Petri, U. Jonas, M. Bach, G. Tovar, K. Mrkvová, M. Vala, J. Homola, W. Knoll, J. Dostálek, *Macromol. Chem. Phys.* **2014**, 215, 2295.
- [29] K. Çaktü, E. Özgür, N. Bereli, A. Denizli, *ChemistrySelect* **2022**, 7, 202200436.
- [30] M. Hussain, K. Kotova, P. A. Lieberzeit, *Sensors* **2016**, 16, 1011.
- [31] S. Roux, B. Garcia, J. L. Bridot, M. Salomé, C. Marquette, L. Lemelle, P. Gillet, L. Blum, P. Perriat, O. Tillement, *Langmuir* **2005**, 21, 2526.
- [32] C. D. Bain, E. B. Troughton, Y. T. Tao, J. Evall, G. M. Whitesides, R. G. Nuzzo, *J. Am. Chem. Soc.* **1989**, 111, 321.
- [33] M. R. Halhalli, C. S. A. Aureliano, E. Schillinger, C. Sulitzky, M. M. Titirici, B. Sellergren, *Polym. Chem.* **2012**, 3, 1033.
- [34] K. Hamase, K. Iwashita, K. Zaitso, *Anal. Sci.* **1999**, 15, 411.
- [35] M. Lehmann, M. Dettling, H. Brunner, G. E. M. Tovar, *J. Chromatogr. B* **2004**, 808, 43.
- [36] Q. Q. Meng, X. Zhao, C. Y. Lin, S. J. Chen, Y. C. Ding, Z. Y. Chen, *Sensors* **2017**, 17, 1846.
- [37] A. Shalabney, I. Abdulhalim, *Opt. Lett.* **2012**, 37, 1175.
- [38] F. O. Ozgur, D. Çimen, A. Denizli, N. Bereli, *Photonic Sens.* **2023**, 13, 230201.
- [39] F. Kolarov, K. Niedergall, M. Bach, G. E. M. Tovar, G. Gauglitz, *Anal. Bioanal. Chem.* **2012**, 402, 3245.
- [40] M. Quaglia, E. De Lorenzi, C. Sulitzky, G. Massolini, B. Sellergren, *Analyst* **2001**, 126, 1495.
- [41] J. M. Lin, T. Nakagama, K. Uchiyama, T. Hobo, *Chromatographia* **1996**, 43, 585.
- [42] J. M. Lin, T. Nakagama, K. Uchiyama, T. Hobo, *Biomed. Chromatogr.* **1997**, 11, 298.
- [43] J. M. Lin, T. Nakagama, K. Uchiyama, T. Hobo, *J. Liq. Chromatogr. Relat. Technol.* **1997**, 20, 1489.
- [44] A. Weber, M. Dettling, H. Brunner, G. E. M. Tovar, *Macromol. Rapid Commun.* **2002**, 23, 824.
- [45] M. M. Titirici, B. Sellergren, *Chem. Mater.* **2006**, 18, 1773.
- [46] A. Farrukh, F. Ashraf, A. Kaltbeitzel, X. Ling, M. Wagner, H. Duran, A. Ghaffar, H. ur Rehman, S. H. Parekh, K. F. Domke, B. Yameen, *Polym. Chem.* **2015**, 6, 5782.
- [47] N. Horn, M. Kreiter, *Plasmonics* **2010**, 5, 331.